Hindawi
Advances in Multimedia
Volume 2023, Article ID 9830470, 1 page
https://doi.org/10.1155/2023/9830470

Retraction

Retracted: Thermal Fault Detection and Diagnosis of Electrical Equipment Based on the Infrared Image Segmentation Algorithm

Advances in Multimedia

Received 15 August 2023; Accepted 15 August 2023; Published 16 August 2023

This article has been retracted by Hindawi following an investigation undertaken by the publisher [1]. This investigation has uncovered evidence of one or more of the following indicators of systematic manipulation of the publication process:

(1) Discrepancies in scope
(2) Discrepancies in the description of the research reported
(3) Discrepancies between the availability of data and the research described
(4) Inappropriate citations
(5) Incoherent, meaningless and/or irrelevant content included in the article
(6) Peer-review manipulation

The presence of these indicators undermines our confidence in the integrity of the article's content and we cannot, therefore, vouch for its reliability. Please note that this notice is intended solely to alert readers that the content of this article is unreliable. We have not investigated whether authors were aware of or involved in the systematic manipulation of the publication process.

Wiley and Hindawi regrets that the usual quality checks did not identify these issues before publication and have since put additional measures in place to safeguard research integrity.

We wish to credit our own Research Integrity and Research Publishing teams and anonymous and named external researchers and research integrity experts for contributing to this investigation.

The corresponding author, as the representative of all authors, has been given the opportunity to register their agreement or disagreement to this retraction. We have kept a record of any response received.

References

[1] H. Li, "Thermal Fault Detection and Diagnosis of Electrical Equipment Based on the Infrared Image Segmentation Algorithm," *Advances in Multimedia*, vol. 2021, Article ID 9295771, 7 pages, 2021.

Hindawi
Advances in Multimedia
Volume 2021, Article ID 9295771, 7 pages
https://doi.org/10.1155/2021/9295771

Research Article

Thermal Fault Detection and Diagnosis of Electrical Equipment Based on the Infrared Image Segmentation Algorithm

Hongzhao Li

Beijing Polytechnic, Beijing 100176, China

Correspondence should be addressed to Hongzhao Li; 101311@bpi.edu.cn

Received 5 August 2021; Accepted 18 October 2021; Published 26 November 2021

Academic Editor: Zhendong Mu

With the advancement of social economy, electricity has gradually entered thousands of households and become a commonly used energy source. However, it cannot be ignored that electricity is dangerous in itself and should be used rationally and effectively. The fault detection of power equipment has become a top priority because they are essential tools for storing, transmitting, and transferring electric power. Based on infrared imaging technology, the principle of infrared imaging technology is introduced in this paper, and effective diagnosis methods are analyzed and summarized in detail. The effectiveness of the proposed infrared image segmentation algorithm is verified through the practical application of the infrared image segmentation algorithm in the detection of interior and exterior faults of electrical equipment.

1. Introduction

The traditional thermal fault detection of power equipment is often carried out depending on manual troubleshooting. On the one hand, it can consume an excessive amount of human resources. On the other hand, the speed and efficiency of emergency response can hardly meet the requirements, and it is difficult to satisfy the needs in the practical situation [1–3]. Therefore, industry experts have introduced infrared thermal imaging technology to carry out fault detection. On the one hand, infrared thermal imaging technology can detect temperature changes of electrical equipment over a long distance accurately. On the other hand, infrared thermal imaging technology can identify electrical equipment failures directly without contact so as to ensure the safety of conventional electric technical inspectors [4, 5]. Firstly, the infrared rays of the object are converted into radiation signals through the optical system, and then the signals are converted into displayable output results by using the analytical electrical signal equipment. In combination with infrared imaging temperature measurement, the temperature changes in the electrical equipment can be detected accurately [6].

This paper attempts to detect and analyze the thermal faults of electrical equipment based on the infrared image segmentation algorithm, with the purpose to maintain the safety and stability of electrical equipment.

2. Infrared Image Segmentation Algorithm

2.1. Blackbody Radiation Law and Infrared Imaging Principle. The so-called blackbody refers to an object that can absorb the incoming radiation at any wavelength. Any object in nature has a certain reflectivity to the incident radiation. In general, blackbody is considered to be idealized models [6–8].

2.2. Infrared Thermal Imager. In terms of the infrared thermal imagers, they can be divided into two types based on the principle of scanning: optical scanning infrared thermal imagers and nonoptical scanning infrared thermal imagers. The principle of the infrared thermal imager based on optical scanning is shown in Figure 1.

Based on the size and image quality of the object to be measured, the infrared radiation is concentrated, filtered, and focused. As long as the speed of the detection instrument is sufficiently high and the response is fast enough, the electric signal proportional to the radiation flux can be

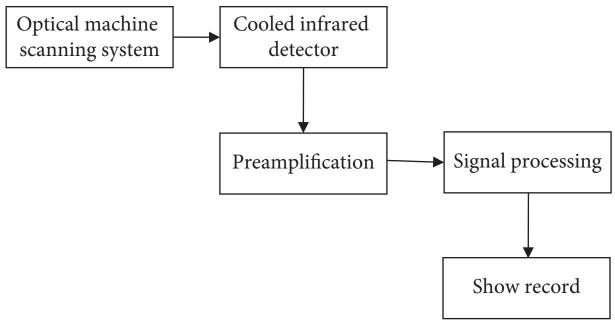

Figure 1: Block diagram of the principle of the infrared thermal imager based on optical mechanical scanning.

detected. The electrical signal is amplified and converted, and the thermal image of the object to be measured is synthesized and presented on the display [9–11].

2.3. Mechanism of Infrared Imaging for the Diagnosis of Thermal Faults. If there is a thermal failure in the electrical equipment, a stable thermal field will be formed, which can radiate energy outward. This abnormal thermal field can be sent back to the display of an infrared imager to generate an infrared thermal image with a thermal field. Based on the distribution of the thermal image, the location of the thermal fault can be identified. In this way, the location of the thermal fault of the equipment can be determined in a timely, effective, and accurate manner.

2.4. Theory of Image Segmentation. In terms of the theory of the image segmentation, it is one of the algorithms based on image segmentation. Its characteristic is that the related pixels are directly associated based on the pixels between the images to complete the mutual conversion between the images. The nodes between the images are identified by sets and expressed as a collection of vertices and edges at the same time, respectively [12]. Firstly, the conversion of the segmented image is carried out, and the pixels in the image are converted into vertices accordingly. The closer the connection between the nodes is, the higher the similarity is. Subsequently, segmentation is carried out based on the connection between edge points and vertices [13, 14].

In the image segmentation based on the algorithm, its characteristic is to optimize the function of the energy. In the algorithm for image segmentation, the object to be measured and the background are segmented effectively. The specific energy consumed by image segmentation is expressed by the following equation:

$$R(f) = E(f) - \lambda B(f). \tag{1}$$

In the above equation, the weight is represented by $E(f)$, which is the energy consumed by segmentation; the area item and boundary term are represented by $R(f)$ and $B(f)$, respectively, and λ is used to stand for the essential relationship between the object to be measured and the boundary term, which indicates the weight of the divided energy. $R(f)$ stands for the attribute of the area item, which can be converted into and represented by pixels specifically, as shown in the following equation:

$$\frac{R(f)}{(f_p)} = \sum_{p\in V} D_p. \tag{2}$$

With respect to the collection of samples with the original point as the background, the specific calculation is shown in equations (3) and (4) as the following:

$$D_p = \frac{-\ln \Pr\left(I_p|\text{“obj”}\right)}{(\text{“obj”})}, \tag{3}$$

$$D_p = \frac{-\ln \Pr\left(I_p|\text{“bkg”}\right)}{(\text{“bkg”})}. \tag{4}$$

The boundary term $B(f)$ is also referred to as the boundary smoothing term. It stands for the attribute of the boundary and is used to evaluate the nonsegmental smoothness of f, which can be calculated based on the following equation:

$$B(f) = \sum_{(p,q)\in N} V_{pq}\left(f_p, f_q\right). \tag{5}$$

In the above equation, N stands for a 4-neighborhood or 8-neighborhood system. The boundary term corresponding to the Potts model can be represented by the following equation:

$$V_{pq}\left(f_p, f_q\right) = \omega_{pq} \times T\left(f_p \neq f_q\right). \tag{6}$$

The calculation of $tg\varphi$ is shown in the following equation:

$$T\left(f_p \neq f_q\right) = \begin{cases} 1, & f_p \neq f_q, \\ 0, & f_p = f_q. \end{cases} \tag{7}$$

The calculation of $\delta_t = (\tau_1 - \tau_2/\tau_1) \times 100\% = (T_1 - T_2/T_1 - T_0) \times 100\%$ is shown in the following equation:

$$\omega_{pq} = e^{-\left(\left|I_p - I_q\right|^2/2\delta^2\right)} \times \frac{1}{\operatorname{dist}(p,q)}. \tag{8}$$

In the above equation, the discontinuous penalty values of pixels p and q are denoted by τ_1; the brightness of pixels p and q is denoted by T_1 and τ_2, respectively; the distance between pixel p and pixel q is denoted by dist (p, q); noise interference is denoted by δ.

2.5. Lazy Snapping Algorithm. In the lazy snapping algorithm, the pixel to be calculated is directly replaced by the pixel block based on the image segmentation algorithm, and its energy calculation equation is shown as follows:

$$\sum_{i\in V} E_1(x_i) = E(X) - \lambda \sum_{(i,j)\in E} E_2\left(x_i, x_j\right). \tag{9}$$

The calculation equation of the area item is shown as the following:

$$\begin{cases} E_1(x_i = 1) = 0 & E_1(x_i = 0) = \infty \\ E_1(x_i = 1) = \infty & E_1(x_i = 0) = 0 \\ E_1(x_i = 1) = \dfrac{d_i^F}{d_i^F + d_i^B} & E_1(x_i = 0) = \dfrac{d_i^F}{d_i^F + d_i^B} \end{cases}$$

$$s.t. \quad \forall i = F, \forall i \in B, \forall i \in U. \tag{10}$$

Equation (10) stands for the calculation method of the regional item energy, in which F stands for the pixels of the foreground (target) point, B stands for the pixels of the background point, and U stands for the pixels of all unconstrained points. The calculation of the area term based on the lazy snapping algorithm and the image segmentation algorithm is more intuitive, and the corresponding extreme value can be obtained. The calculation of the boundary term is shown as the following:

$$E_2(i, j) = \frac{\left|x_i - x_j\right|}{\varepsilon + \|C(i) - C(j)\|^2}. \tag{11}$$

In the above equation, the brightness of the adjacent pixel i and pixel j can be represented by $C(i)$ and $C(j)$, respectively; ε is the adjustment parameter (the default value is 1).

3. Criteria for the Detection and Diagnosis of Thermal Faults of Electrical Equipment

3.1. Heat Source. With respect to electrical equipment, due to the effects of voltage and current, three main sources of heat energy will be produced in general:

(1) Heating of electrical equipment: based on the Ampere–Joule theorem, when current passes through the electrical equipment, heat will be generated. At this point, a huge amount of current is observed in current-carrying equipment.

(2) With regard to the heating due to the continuous change in the polarization direction of the medium and the consumption of electric energy, the electric power consumed due to heating is shown as follows:

$$P = U^2 \omega C tg\varphi. \tag{12}$$

In the above equation, the voltage is represented by U, the AC voltage angular frequency is represented by ω, the equivalent capacitance of the medium is represented by C, and the dielectric loss tangent is represented by $tg\varphi$.

(3) Due to the hysteresis and eddy current of the iron core, electrical energy loss is produced, and heat is generated.

3.2. Types of Faults. The faults of electrical equipment can be divided into exterior and interior faults based on infrared diagnosis. (1) Where there is an exterior thermal infrared failure, infrared rays radiate to the surroundings in the form of local overheating. For example, the infrared thermal image at the joint of the conductive wire presents a thermal image distribution with the fault point as the center. Based on the thermal image, it can be distinguished whether there is a thermal fault so that the temperature distribution can be accurately identified accordingly. (2) Where there is an interior thermal failure, the heating process is relatively long, which can change the exterior thermal field distribution of the equipment. Hence, through the inspection and analysis of the infrared thermal image, the interior failure of the equipment can be detected and diagnosed.

3.3. Criteria for Diagnosis. As shown in Figure 2, the criteria for the detection of exterior thermal faults can be calculated.

The ratio of the temperature difference between the two corresponding measuring points with the same or essentially the same condition in the two pieces of equipment to the temperature rise of a measuring point with a higher temperature can be calculated based on the following equation:

$$\delta_t = \frac{\tau_1 - \tau_2}{\tau_1} \times 100\%, \tag{13}$$

$$\delta_t = \frac{T_1 - T_2}{T_1 - T_0} \times 100\%. \tag{14}$$

In the above equation, the temperature rise and temperature at the heating point are represented by τ_1 and T_1, respectively; the temperature rise and temperature corresponding to the normal equipment are represented by τ_2 and T_2, respectively; and the ambient temperature is represented by T_0.

When $\delta_t > 35\%$, the defects in the equipment can be diagnosed.

4. Detection and Diagnosis Simulation of Exterior Thermal Faults of Electrical Equipment

4.1. Thermal Fault Detection and Diagnosis of the Insulator String. With respect to insulators, the fault detection of string heating is to determine whether there is a fault based on the temperature field image of the whole insulator string, instead of making judgment based on the temperature of the insulator. In accordance with the previous studies, the temperature distribution on the ceramic cap of a good insulator string corresponds to its distribution. In this way, insulators with poor quality can be identified. The insulators with high temperature are inferior.

4.2. Fault Detection and Diagnosis of the Cable Based on Infrared Imaging. The interior faults of the cable include poor contact, and its thermal characteristics are determined based on the overheating on the surface of the defect or the overall overheating. The maximum allowable temperature rise of the cable can be used to determine whether there is failure by using the phase-to-phase method.

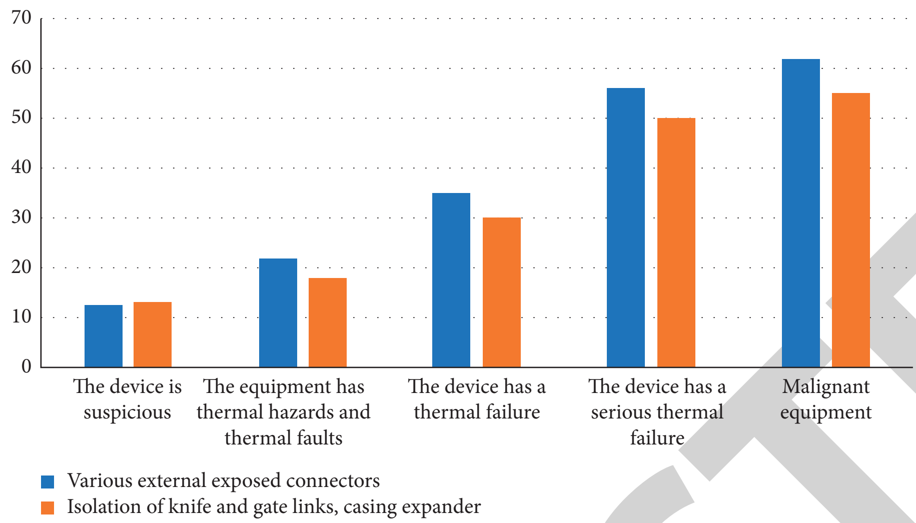

Figure 2: Criteria for the detection of exterior thermal faults (temperature difference between the hot spot and lowest temperature point) (°C).

4.3. Interior Thermal Fault Detection and Diagnosis of the Switch. The thermal field distribution of the switch housing is determined by using the method of comparing the resistance of the conductive loop and the ferromagnetic loss with each other in the horizontal and vertical directions. If the temperature is abnormal, the possible fault points are determined based on the differences in the comparison results. If there is a switch for 10 kV, a thermal image is taken in the three-phase group at the same time, and the difference between the highest and the lowest temperature is more than 5°C. At this point, it can be considered as an interior thermal fault. If the difference between the highest and the lowest temperature is at 2-3°C, it should be tracked and monitored accordingly. If the difference between the highest and the lowest temperature is more than 10°C, the power should be cut off for the corresponding treatment.

4.4. Interior Thermal Fault Detection and Diagnosis of the Current Transformer. The current transformer loss is composed of the copper loss, the iron loss, and the joint resistance loss, which are dissipated in the form of heat at the top cap. The method of horizontal and vertical comparison is used to determine the fault based on the criteria as the following: the interphase temperature difference is more than 20°C, and the one at a high temperature has severe interior thermal failure; where the temperature difference is more than 15°C, the power supply should be cut off for testing and inspection; where the temperature difference is more than 10°C, the monitoring should be strengthened; in addition, the temperature rise relative to the environment should not be greater than 70°C.

4.5. Cases of the Contact Thermal Fault

4.5.1. Infrared Temperature Measurement Process. In practical work, infrared preheating is used to carry out simulation, and it is found that there is an overheating phenomenon in the A3 capacitor of the 10 kV #9 capacitor bank. After infrared detection, it is found based on infrared image segmentation algorithm that the A-phase busbar of the #9 capacitor bank is overheated, the highest temperature of the heating point is 62.3°C, the ambient temperature is 25°C, the humidity is 65%, and the heating point is 37.3°C higher in temperature relative to the indoor environment temperature of the capacitor.

For the purpose of further analysis, the infrared thermal fault spectrum is loaded into infrared analysis software for visual display in this paper.

4.5.2. Infrared Analysis of the Characteristic Spectrum. The results indicate that the highest temperature of the entire spectrum is 63.5°C at the junction of the $A3$ capacitor fuse and the busbar. The highest temperature of the adjacent capacitors $A2$ and $A4$ and the busbar connection area ($C2$ and $C1$, respectively) on the left and right sides is 37.2°C and 39.1°C, respectively, which are introduced into the calculation equation of relative temperature difference as follows:

$$\partial = \frac{(T_1 - T_2)}{(T_1 - T_0)} \times 100\%. \tag{15}$$

In the above equation, T_1 stands for the temperature of the heating point, T_2 stands for the temperature of the normal corresponding point, and T_0 stands for the ambient temperature.

In the equation, the relative temperature difference between the heating point and the corresponding part is shown in Figure 3.

It can be observed from Figure 3 that the relative temperature difference of the junction between the capacitor fuse $A3$ and the busbar from the abnormal heating part A corresponding to the normal temperature and the junction between the capacitor fuse and the busbar and the relative temperature difference between the $A4$ capacitor fuse and the busbar are about 68% and 63%, respectively. Hence, it

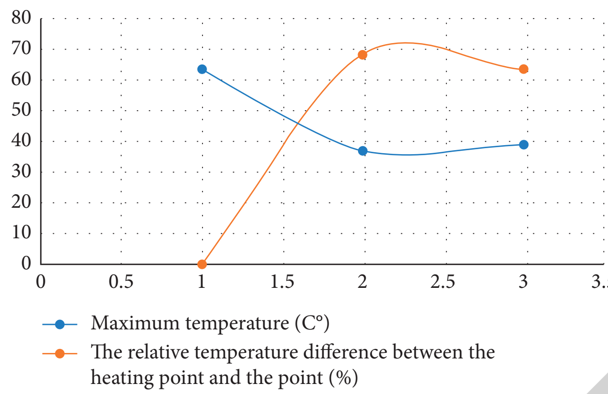

Figure 3: Table of the relative temperature difference between the abnormal heating point and the corresponding normal temperature part.

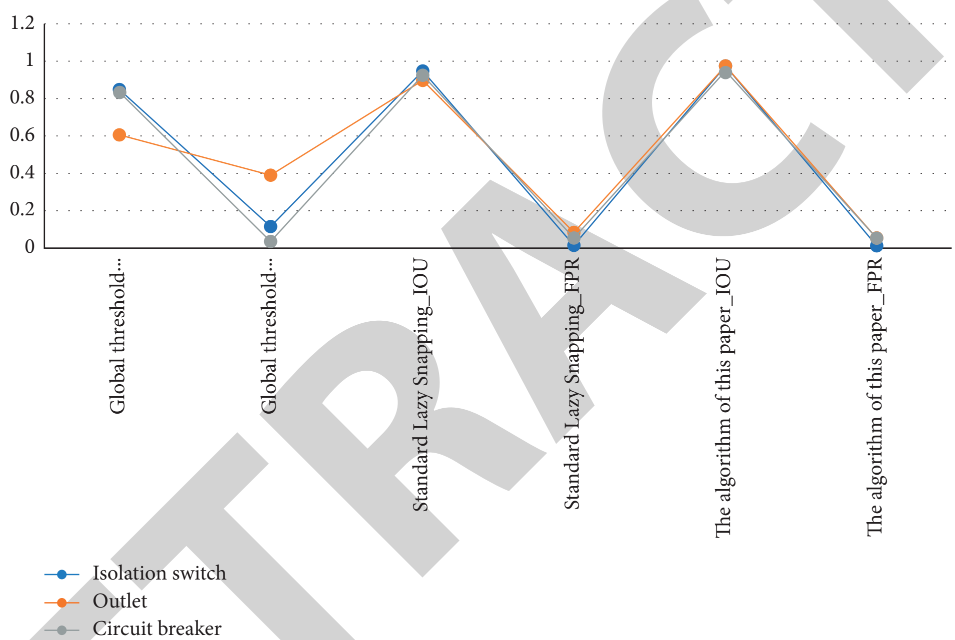

Figure 4: Segmentation effects of various types of infrared images.

can be determined that this abnormal heating phenomenon is a general defect in the infrared temperature measurement.

4.5.3. Treatment of the Defects. After inspection by the maintenance personnel, it is found that the *A*3 capacitor fuse in the 10 kV #9 capacitor bank and the busbar connection screw are seriously worn out. In addition, the surface of the busbar reacts with air and forms a layer of oxide film under long-term operating conditions, resulting in poor connection between the *A*3 capacitor fuse and the busbar and excessive heat generation during the operation.

4.6. Case Analysis of Equipment Aging and Heating

4.6.1. Infrared Temperature Measurement Process. During the process that high-voltage technical personnel are carrying out infrared temperature measurement in the test, the power outage test for abnormal heating is inspected. The results indicate that insulation resistance of each secondary terminal of the voltage transformer to the ground is 500 MΩ only. The insulation resistance of the low-voltage terminal (N) of the capacitive voltage transformer and the low-voltage terminal (XL) of the intermediate transformer to the ground is less than 2 MΩ. Thus, it is necessary to return the voltage transformer to the factory for further inspection.

4.6.2. TYD Return to Factory Test Situation. Before the disassembly, the technicians performed an oil test and a conventional high-voltage test on the TYD in turn and found that the oil samples, coupling capacitors, and intermediate transformers were all functioning normally. However, there were problems in the secondary auxiliary winding damper unit of the intermediate transformer, specifically the deterioration of the damper capacitance, which causes the electromagnetic unit to heat up.

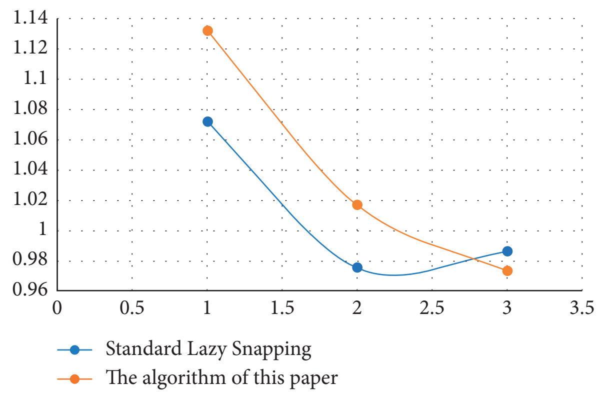

Figure 5: Comparison of algorithm running time.

4.6.3. Conclusion of Return to Factory Test. To sum up, due to water seepage in the secondary terminal box of the 220 kV Bingjiang station 110 kV 3M bus TYD, it leads to the situation that some secondary terminals become damp and corroded, resulting in a relatively huge leakage current, which causes the secondary terminal box to heat up. At the same time, due to the aging of the capacitive element, the power frequency resonance condition of the secondary auxiliary winding damper of the voltage transformer is damaged. As a result, the power frequency current that flows through the damper increases sharply, causing the upper fuel tank of the electromagnetic unit of the voltage transformer to heat up.

From the results in Figure 4, it can be seen that the two indicators of IOU and FPR after segmentation based on the algorithm put forward in this paper are the highest and the lowest, respectively. This suggests that the segmentation accuracy of the algorithm proposed in this paper is relatively high and can make certain segmentation corrections to the algorithm, indicating that there are also evident improvements in the segmentation effect, which has improved the segmentation efficiency and enhanced the segmentation effect. From Figure 5, it can be clearly observed that the overall running speed of the algorithm put forward in this paper performs in the direction of the presegmentation link which can ensure that the algorithm can meet the requirements for high real-time performance.

5. Conclusions

The inspection of electrical equipment is not only one of the top priorities but also an essential way to ensure the safety of manual inspection. In this paper, the thermal faults of electrical equipment are detected and diagnosed based on the infrared image segmentation algorithm, with the purpose to analyze the reliability and effectiveness of electrical equipment and improve the economic benefits of their operation. The correctness of the proposed method is verified through the practical application of thermal infrared imaging technology in the detection of thermal faults.

Data Availability

The data used to support the findings of this study are available upon request to the author.

Conflicts of Interest

The author declares no conflicts of interest.

Acknowledgments

This paper was supported by the Project Based on the School-Level Scientific and Technological Key Subject which is titled Research on the Thermal Fault Detection System of Electrical Equipment Based on Image Feature Analysis (2017Z004-013-KXZ).

References

[1] A. Dakkoune, L. Vernières-Hassimi, D. Lefebvre, and L. Estel, "Early detection and diagnosis of thermal runaway reactions using model-based approaches in batch reactors," *Computers & Chemical Engineering*, vol. 140, no. 18, pp. 106–112, 2020.

[2] A. Berzoy, H. H. Eldeeb, and O. A. Mohammed, "On-line detection of stator faults in DTC-driven IM using SC impedance matrix off-diagonal term," *IEEE Transactions on Industry Applications*, vol. 55, no. 6, pp. 5906–5915, 2019.

[3] C. Hu, S. He, and Y. Wang, "A classification method to detect faults in a rotating machinery based on kernelled support tensor machine and multilinear principal component analysis," *Applied Intelligence*, vol. 5, no. 2, pp. 56–63, 2020.

[4] M. A. Thompson, J. C. Ford, and G. R. Long, "On-line detection in slab gel electrophoresis using thermal lens spectrophotometry," *Applied Spectroscopy*, vol. 46, no. 6, pp. 234–242, 2016.

[5] M. Emil, "Potential of the flowing eluent wall and aliquot on-line detection in the OPLC 50 and 100 systems," *JPC—Journal of Planar Chromatography—Modern TLC*, vol. 21, no. 2, pp. 97–102, 2015.

[6] F. Cai, H. Li, Y. Tian et al., "Erratum: electrical detection and analysis of surface acoustic wave in line-defect two-dimensional piezoelectric phononic crystals," *Japanese Journal of Applied Physics*, vol. 57, no. 5, pp. 592–600, 2018.

[7] C. A. Hepburn, P. Vale, A. S. Brown, N. J. Simms, and E. J. McAdam, "Development of on-line FTIR spectroscopy for siloxane detection in biogas to enhance carbon contactor management," *Talanta*, vol. 141, no. 3, pp. 128–136, 2015.

[8] H. Chen, B. Jiang, W. Chen, and H. Yi, "Data-driven detection and diagnosis of incipient faults in electrical drives of high-speed trains," *IEEE Transactions on Industrial Electronics*, vol. 2, no. 6, pp. 101–110, 2018.

[9] J. M. Andújar a, F. Segura, F. Isorna, and A. J. Calderón, "Comprehensive diagnosis methodology for faults detection and identification, and performance improvement of air-cooled polymer electrolyte fuel cells," *Renewable and Sustainable Energy Reviews*, vol. 88, no. 3, pp. 193–207, 2018.

[10] H. Zou and F. Huang, "A novel intelligent fault diagnosis method for electrical equipment using infrared thermography," *Infrared Physics & Technology*, vol. 73, no. 3, pp. 29–35, 2015.

[11] H. Cui, S. Huo, H. Ma, W. Guo, C. Ge, and L. Qin, "Effects of view angle and measurement distance on electrical equipment

UV corona discharge detection," *Optik*, vol. 171, no. 2, pp. 672–677, 2018.
[12] G. Faure, M. Vallée, C. Paulus, and T. Q. Tran, "Fault detection and diagnosis for large solar thermal systems: a review of fault types and applicable methods," *Solar Energy*, vol. 197, no. 2, pp. 472–484, 2020.
[13] S. T. Lee and H. Jin, "Detection technique for stator inter-turn faults in BLDC motors based on third harmonic components of line currents," *IEEE Transactions on Industry Applications*, vol. 53, no. 1, pp. 143–150, 2015.
[14] F. Tahir, M. T. Islam, J. Mack, J. Robertson, and D. Lovett, "Process monitoring and fault detection on a hot-melt extrusion process using in-line raman spectroscopy and a hybrid soft sensor," *Computers & Chemical Engineering*, vol. 125, no. 9, pp. 400–414, 2019.